CHEMISTRY
A EUROPEAN JOURNAL

DOI: 10.1002/chem.200500752

Electron-Rich Diferrous–Phosphane–Thiolates Relevant to Fe-only Hydrogenase: Is Cyanide "Nature's Trimethylphosphane"?

Jarl Ivar van der Vlugt, Thomas B. Rauchfuss,* and Scott R. Wilson[a]

Abstract: The two-step one-pot oxidative decarbonylation of $[Fe_2(S_2C_2H_4)(CO)_4(PMe_3)_2]$ (**1**) with $[FeCp_2]PF_6$, followed by addition of phosphane ligands, led to a series of diferrous dithiolato carbonyls **2**–**6**, containing three or four phosphane ligands. In situ measurements indicate efficient formation of $\mathbf{1}^{2+}$ as the initial intermediate of the oxidation of **1**, even when a deficiency of the oxidant was employed. Subsequent addition of PR_3 gave rise to $[Fe_2(S_2C_2H_4)(\mu\text{-}CO)(CO)_3(PMe_3)_3]^{2+}$ (**2**) and $[Fe_2(S_2C_2H_4)(\mu\text{-}CO)(CO)_2(PMe_3)_2(PR_3)_2]^{2+}$ (R = Me **3**, OMe **4**) as principal products. One terminal CO ligand in these complexes was readily substituted by MeCN, and $[Fe_2(S_2C_2H_4)(\mu\text{-}CO)(CO)_2(PMe_3)_3(MeCN)]^{2+}$ (**5**) and $[Fe_2(S_2C_2H_4)(\mu\text{-}CO)(CO)(PMe_3)_4(MeCN)]^{2+}$ (**6**) were fully characterized. Relevant to the H_{red} state of the active site of Fe-only hydrogenases, the unsymmetrical derivatives **5** and **6** feature a semibridging CO ligand *trans* to a labile coordination site.

Keywords: hydrogenases · iron · phosphanes · thiolates

Introduction

Research on the chemistry of diiron–carbonyl–dithiolates, $[Fe_2(\mu\text{-}SR)_2(CO)_6]$, dates back to the 1920s with the preparation of the ethanethiol derivative.[1,2] Decades of subsequent work have demonstrated the versatility of this motif. Recently, various states for the active site of the Fe-only hydrogenase enzymes were spectroscopically and structurally characterized and shown to contain strongly related diiron–carbonyl–thiolates.[3–5] The structural biology presents many challenges to the basic chemistry of the diiron–dithiolates,[6] including coordination of a 4Fe-4S cluster, a novel dithiolate cofactor,[7] and the occurrence of CN^- ligands. Many of these features are being addressed in an effort to develop structural and functional models for Fe-only hydrogenases active site.[8] Quite apart from biomimetic H_2 production, the structural features found in the enzyme active site indicate that the diiron–dithiolate framework is more versatile than previously appreciated. It is in this spirit that we have undertaken an investigation of the diferrous–phosphane–thiolates described herein.

[a] Dr. J. I. van der Vlugt, Prof. Dr. T. B. Rauchfuss, Dr. S. R. Wilson
Department of Chemistry
University of Illinois at Urbana-Champaign
505 S. Mathews St., Urbana, IL 61801 (USA)
Fax: (+1) 217-333-2685
E-mail: rauchfuz@scs.uiuc.edu

Several structural[9] and functional aspects[10–12] of the Fe-only hydrogenases active site have been successfully modeled in the past five years, but with a few notable exceptions,[13,14] all studies focused on classical $[Fe^I]_2$ species or their protonated derivatives, which are formally diferrous.

We have developed an oxidative decarbonylation route to synthesize well-defined diferrous–dithiolates.[15] Oxidative decarbonylation, which entails concomitant oxidation and ligand substitution at a metal carbonyl, is a reasonably well-established methodology,[16–21] and it represents a versatile entry into species of bioinorganic interest. For example, this approach led to the series $[Fe_2(SR)_2(\mu\text{-}CO)(CO)_x(CNMe)_{6-x}]^{2+}$ (Figure 1), which are good structural mimics of the H_{ox}^{air} state of the Fe-only hydrogenase active site.[22] A recent extension of the oxidative decarbonylation methodology led to the diferrous–dicyanide $[Fe_2(S_2C_2H_4)(\mu\text{-}CO)(CN)_2(CO)_2(PMe_3)_2]$ (Figure 1).[23] During these investigations, we realized that the bisphosphane $[Fe_2(S_2C_2H_4)(CO)_4(PMe_3)_2]$ (**1**), with an $E_{1/2}$ of 350 mV versus Ag/AgCl, should be oxidizable by $[FeCp_2]^+$. Indeed, treatment of **1** with two equivalents of $[FeCp_2]PF_6$ and two equivalents of Et_4NCN yielded another isomer of $[Fe_2(S_2C_2H_4)(\mu\text{-}CO)(CN)_2(CO)_2(PMe_3)_2]$ (Figure 1).[23]

The specific issue that we begin to address is the complicated reactivity of cyanide, the naturally occurring donor ligand that supports the active site of the Fe-only hydrogenases. In particular, the oxidation and protonation of the cyano derivatives has proven difficult because of the high

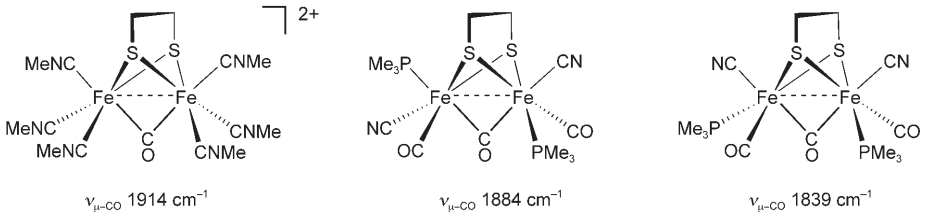

Figure 1. Structures of various complexes discussed.

reactivity inherent in this bifunctional ligand,[24] that is, the ability of Fe*CN* to bridge to other metals and the Brønsted basicity of the Fe*CN* fragment. In the natural protein, these complications are minimized by a combination of site isolation, which precludes formation of Fe-CN-Fe bridges, and hydrogen bonding,[4] which diminishes the basicity of the Fe*CN* group. In view of these complications, PMe_3 represents an attractive replacement for cyanide. As we demonstrate, the preparative chemistry of the $Fe_2(SR)_2$-PMe_3-CO system is rich and efficient. To simplify the spectroscopic and structural analyses, we focused on ethanedithiolate derivatives. The main results are summarized in Scheme 1.

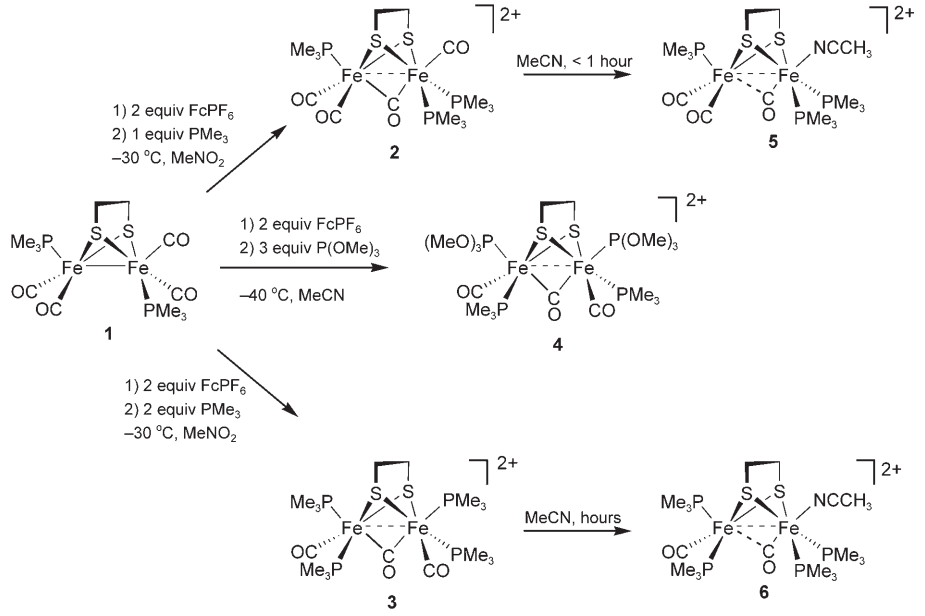

Scheme 1. Synthetic routes to **2**–**6** via oxidative decarbonylation of **1** with $[FeCp_2]PF_6$ and additional trapping ligands.

Results and Discussion

Synthesis of $[Fe_2(S_2C_2H_4)(\mu\text{-CO})(CO)_{2+x}(PR_3)_{4-x}](PF_6)_2$ (x=0, 1): Low-temperature oxidation of $[Fe_2(S_2C_2H_4)(CO)_4(PMe_3)_2]$ (**1**) in neat $MeNO_2$ in the presence of one equivalent of PMe_3 gave the red salt $[Fe_2(S_2C_2H_4)(\mu\text{-CO})(CO)_3(PMe_3)_3](PF_6)_2$ (**2**). ^{31}P NMR and IR spectra of this species (Figure 2a) indicated a structure with C_s symmetry.

Oxidation of solutions of **1** in $MeNO_2$ in the presence of two equivalents of PMe_3 gave the tetraphosphane $[Fe_2(S_2C_2H_4)(\mu\text{-CO})(CO)_2(PMe_3)_4](PF_6)_2$ (**3**). This red salt is characterized by two equally intense doublets of doublets in the ^{31}P NMR spectrum, consistent with C_2 symmetry. The $J_{P,P}$ coupling constants of 49 and 6 Hz are assigned to two- and three-bond couplings, respectively. The IR spectrum showed a strong band for ν_{CO} at 2001 cm^{-1}, accompanied by a shoulder at 2013 cm^{-1} and a weak, broad band attributable to $\nu_{\mu\text{-CO}}$ at 1840 cm^{-1}, consistent with a single C_2-symmetric species. The structure of **3** was verified crystallographically (see below).

Oxidation of **1** with $[FeCp_2]PF_6$ in cold MeCN and subsequent addition of three equivalents of $P(OMe)_3$ cleanly formed red-brown $[Fe_2(S_2C_2H_4)(\mu\text{-CO})(CO)_2(PMe_3)_2(P(OMe)_3)_2](PF_6)_2$, (**4**), which was characterized by NMR and IR spectroscopy (Figure 2b), ESI-MS, and X-ray crystallography. The spectroscopic data for even the crude reaction product clearly suggest formation of a single isomer of **4**, with no indication of any MeCN incorporated (vide infra). Tellingly, the ^{31}P NMR spectrum featured two doublets of doublets patterns, consistent with a structure analogous to that for tetraphosphane **3**. The IR patterns for **3** and **4** in the carbonyl region are similar, although the bands for **4** were shifted by 14–23 cm^{-1} to higher energy. The alternative pathway to **4**, by oxidation of the bis(phosphite) $[Fe_2(S_2C_2H_4)(CO)_4(P(OMe)_3)_2]$ with $[FeCp_2]PF_6$ and addition of PMe_3, is not accessible because the oxidation potential of this bis(phosphite) species is too high, at ≈685 mV versus Ag/AgCl.

MeCN adducts of diferrous–dithiolates: Red solutions of trisphosphane **2** became dark green in the presence of MeCN, due to formation of $[Fe_2(S_2C_2H_4)(\mu\text{-CO})(CO)_2(PMe_3)_3(MeCN)](PF_6)_2$ (**5**). The ^{31}P NMR spectrum of **5** showed a triplet and a doublet in a 1:2 ratio, with $J_{P,P}$≈6 Hz, consistent with three-bond coupling across the Fe–Fe bond. The bridging CO ligand appeared as a doublet of triplets in the ^{13}C NMR spectrum at δ=218 ppm. In addition to bands for terminal CO ligands, the IR spectrum showed a weak, broad band at 1908 cm^{-1}, assigned to μ-CO (Figure 2c). The compound was further characterized by X-ray crystallography (see below). Interestingly,

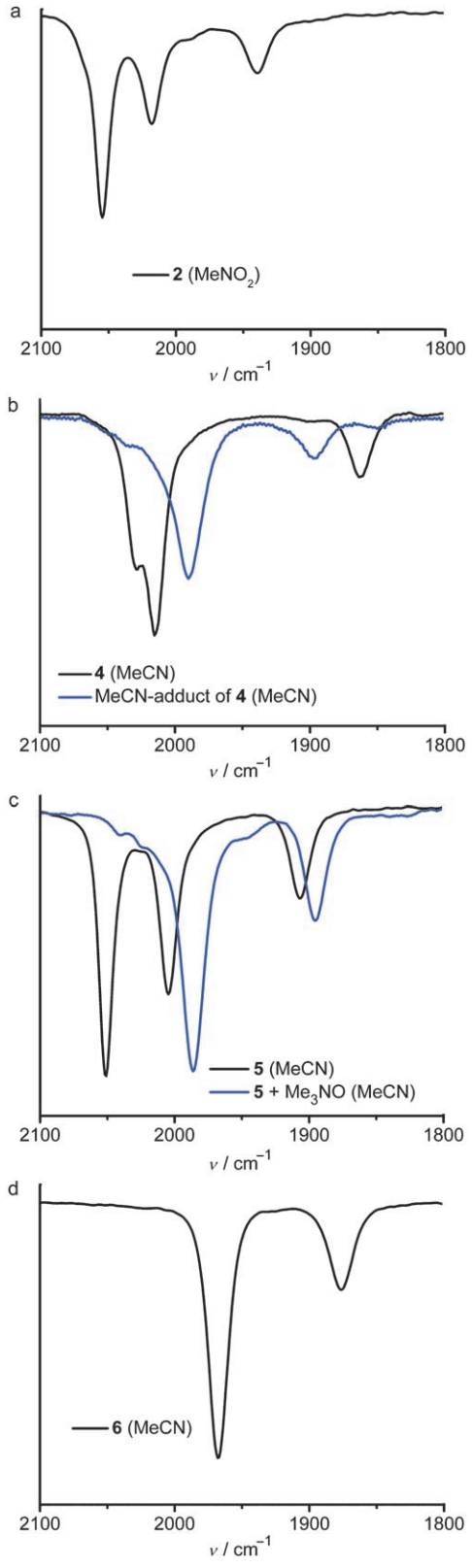

Figure 2. FT-IR spectra, carbonyl region, of diferrous phosphino thiolates **2**–**6** (solvent in brackets).

the CO ligand that is displaced by the MeCN ligand is coordinated in the axial position, *trans* to the μ-CO ligand, as deduced from the spectroscopic similarities between **2** and **5**.

We serendipitously prepared the EtCN analogue of **5** by means of oxidation of **1** with $[FeCp_2]PF_6$ in unpurified $MeNO_2$, which is known to be contaminated with EtCN.[25] Thus, **2** is highly reactive towards even traces of nitrile in solution. Upon stirring in neat EtCN at room temperature, **5** exchanged its MeCN ligand for EtCN, as monitored by ^{31}P NMR spectroscopy, which showed a shift $\Delta\delta$ of 0.6 ppm for the two doublets. The MeCN ligand in complex **5** was not displaced by CO (1 atm) in neat $MeNO_2$, even at 50 °C.

When the oxidative decarbonylation of **1** was followed by addition of one equivalent of PMe_2Ph in place of PMe_3, followed by a room-temperature workup, we obtained the mixed ligand complex $[Fe_2(S_2C_2H_4)(\mu\text{-}CO)(CO)_2(PMe_3)_2(PMe_2Ph)(MeCN)](PF_6)_2$. IR and ^{31}P NMR spectra indicate that this mixed phosphane species is structurally analogous to **5**, with the PMe_2Ph fragment residing in a basal position on the Fe center bearing both PMe_3 and MeCN ligands. This species is presumed to arise via the intermediacy of $[Fe_2(S_2C_2H_4)(\mu\text{-}CO)(CO)_3(PMe_3)_2(PMe_2Ph)](PF_6)_2$.

Treatment of a solution of **5** in either $MeNO_2$ or MeCN with one equivalent PMe_3 instantaneously and efficiently yielded compound **3**. The conversion was signaled by a color change from dark green to red, as well as by the appropriate changes in the ^{31}P NMR and IR spectra. The electrophilicity of the terminal CO ligands in **5** was also evidenced by the rapidity of the low-temperature reaction of **5** with the decarbonylation agent Me_3NO in MeCN. The IR spectrum of the product, proposed to be $[Fe_2(S_2C_2H_4)(\mu\text{-}CO)(CO)(PMe_3)_3(MeCN)_2](PF_6)_2$, consisted of two ν_{CO} bands (1987 and 1895 cm^{-1}), the latter being assigned to μ-CO (Figure 2c).

The solvolysis of **3** in MeCN proceeded approximately ten times more slowly than the solvolysis of **2**, and the product was $[Fe_2(S_2C_2H_4)(\mu\text{-}CO)(CO)(PMe_3)_4(MeCN)](PF_6)_2$ (**6**), as supported by the observation of two CO bands in the IR spectrum (Figure 2d). ^{31}P NMR spectroscopy indicated that **6** exists as a single diastereomer, in which all four PMe_3 ligands are nonequivalent, in contrast to the high symmetry of **3**. The molecular structure of **6** was corroborated by X-ray crystallography (see below). Compound **6** could also be conveniently prepared by means of a one-pot reaction involving oxidative decarbonylation of **1** in MeCN, followed by addition of three equivalents PMe_3. When the conversion of **3** into **6** was monitored by using ^{31}P NMR spectroscopy, we observed an intermediate, labeled **A**. This low-symmetry species is most likely isomeric with **6**. The proposed mechanism for the conversion of **3** to **6** is depicted in Scheme 2.

In contrast to the solvolysis of **3**, solutions of $[Fe_2(S_2C_2H_4)(\mu\text{-}CO)(CO)_2(PMe_3)_2(P(OMe)_3)_2](PF_6)_2$ (**4**) in MeCN required days even at 50 °C for substitution of one CO ligand by MeCN (Figure 2b). The major product ($\approx$85 %) of this solvolysis is proposed to have $P(OMe)_3$ and MeCN ligands in the axial positions, similar to species **6**, as deduced from ^{31}P NMR and FT-IR spectroscopy, combined with the apparent preference for $P(OMe)_3$ to occupy the

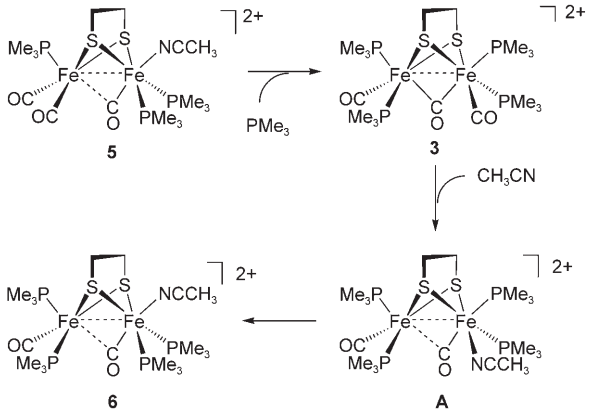

Scheme 2. Postulated pathway for the conversion of **5** via **3** to **6**.

axial position *trans* to the Fe–Fe bond (vide infra). The ^{31}P NMR spectrum showed four multiplets at $\delta = 160.7$ (79 Hz), 139.8 (53 Hz), 26.2 (53 Hz) and 15.0 ppm (79 Hz), with phosphane–phosphite two-bond coupling constants indicated in parentheses. The ^{31}P NMR and IR spectroscopic data for compounds **2**–**6** are given in Table 1.

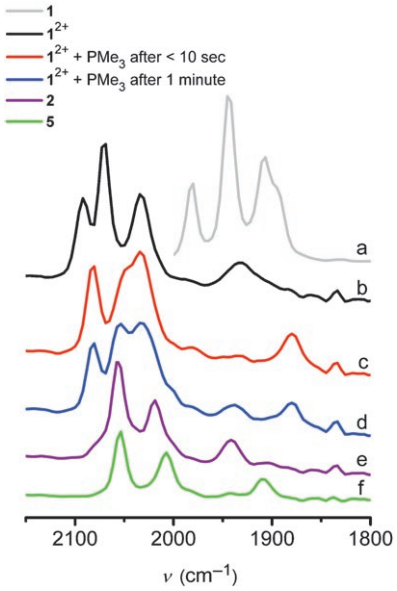

Figure 3. In situ ATR-IR spectra (carbonyl region, $MeNO_2$): a) compound **1** at −30 °C; b) addition of two equivalents $[FeCp_2]PF_6$ at −30 °C to give $\mathbf{1}^{2+}$; c) addition of one equivalent PMe_3 at −30 °C; d) same solution after 1 minute at −30 °C; e) same solution after five minutes at −30 °C; f) 30 minutes after addition of ≈25 equivalents MeCN at room temperature.

Table 1. ^{31}P NMR and FT-IR spectroscopic data for compounds **2**–**6** (P = PMe_3).

Compound	^{31}P [ppm] {$J_{P,P}$ [Hz]}	ν_{CO} [cm^{-1}]
$[Fe_2(S_2C_2H_4)(\mu\text{-}CO)(CO)_3(P)_3]^{2+}$ ($\mathbf{2}^{2+}$)	39.8, 24.1 {6}	2055, 2019, 1942
$[Fe_2(S_2C_2H_4)(\mu\text{-}CO)(CO)_2(P)_4]^{2+}$ ($\mathbf{3}^{2+}$)	21.0, 19.7 {49, 6}	2013, 2001, 1840
$[Fe_2(S_2C_2H_4)(\mu\text{-}CO)(CO)_2(P)_2(P(OMe)_3)_2]^{2+}$ ($\mathbf{4}^{2+}$)	143.4, 21.3 {89, 6}	2028, 2015, 1863
$[Fe_2(S_2C_2H_4)(\mu\text{-}CO)(CO)_2(P)_3(MeCN)]^{2+}$ ($\mathbf{5}^{2+}$)	35.9, 27.5 {6}	2054, 2007, 1909
$[Fe_2(S_2C_2H_4)(\mu\text{-}CO)(CO)(P)_4(MeCN)]^{2+}$ ($\mathbf{6}^{2+}$)	32.7, 24.5, 14.6, 14.1 {41, 29, 6, 3}	1969, 1878

Studies on the oxidative decarbonylation process: The oxidation of **1** with $[FeCp_2]^+$ in MeCN was examined by in situ IR spectroscopy at −40 °C. Upon addition of two equivalents of $[FeCp_2]PF_6$, new ν_{CO} bands appeared instantaneously at 2092, 2069, 2030 and 1934 cm^{-1}. The overall pattern is similar to that for **1**, but shifted by ≈100–150 cm^{-1} to higher frequency (Figure 3). This species, labeled $\mathbf{1}^{2+}$, formed irrespective of a CO atmosphere and was found to be stable at −40 °C for extended periods. Efficient formation of species $\mathbf{1}^{2+}$ was also obtained for the oxidative decarbonylation in neat $MeNO_2$, again regardless of the presence of CO. We propose that $\mathbf{1}^{2+}$ is the unsaturated diferrous species $[Fe_2(S_2C_2H_4)(CO)_4(PMe_3)_2]^{2+}$. Oxidation of **1** with one equivalent $[FeCp_2]PF_6$ yielded a 1:1 mixture of **1** and $\mathbf{1}^{2+}$. Further investigations into the nature of this species are ongoing.

Treatment of $\mathbf{1}^{2+}$ with one equivalent PMe_3 at low temperatures led to a color change from brown-red to dark red; concomitantly, peaks corresponding to **2** appeared, at the expense of peaks for $\mathbf{1}^{2+}$. A transient intermediate was observed prior to the formation of **2** with a μ-CO band at ≈1875 cm^{-1} (Figure 3). This species is short-lived, as compound **2** is the major species within a few minutes, even at low temperatures. Based on IR data, **2** is stable in neat $MeNO_2$, but upon addition of MeCN (≈25 equiv, room temperature), compound **2** was cleanly converted into **5**, a reaction that requires 30 min. (Figure 3).

X-ray crystallography: The overall molecular structures of the crystallographically characterized compounds **3**–**6** are relatively similar (Figure 4, Table 2). Each consisted of a face-sharing bioctahedral core, not unlike previous members of this series of diferrous–dithiolates, that is, $[Fe_2(S_2C_2H_4)(\mu\text{-}CNMe)(CNMe)_6]^{2+}$,[15] $[Fe_2(S_2C_2H_4)(\mu\text{-}CO)(CNMe)_6]^{2+}$,[22] and $[Fe_2(S_2C_2H_4)(\mu\text{-}CO)(CN)_2(CO)_2(PPh_3)_2]$.[23] The Fe–Fe distances fall in the range 2.5135(12)–2.6006(7) Å, comparable to other diferrous–thiolates as well as the Fe-only hydrogenase active site.[4,26] The bridging CO ligand in **3** and **4** is coordinated in a symmetric fashion, indicated by the similar bond lengths for Fe1–C1 and Fe2–C1 in each case. In contrast, notable differences are observed for the Fe–C(1) distances in **5** (2.407(4) and 1.775(4) Å) and **6** (2.322(3) and 1.779(3) Å), with the values for Fe2–C1 very close to the bond lengths observed for terminal CO ligands. This asymmetry in the binding of the μ-CO clearly indicates that this CO ligand is coordinated in a semibridging fashion.[27,28] Correspondingly, the Fe1–P1 bond length is slightly shortened in **5** and **6** (2.216(2)–2.2295(9) Å) relative to that found in **3** (Fe1–P1 is 2.285(2) Å). The Fe–Fe bond lengths are noticeably longer (2.56–2.60 Å) for the unsymmetrical complexes **5** and **6**.

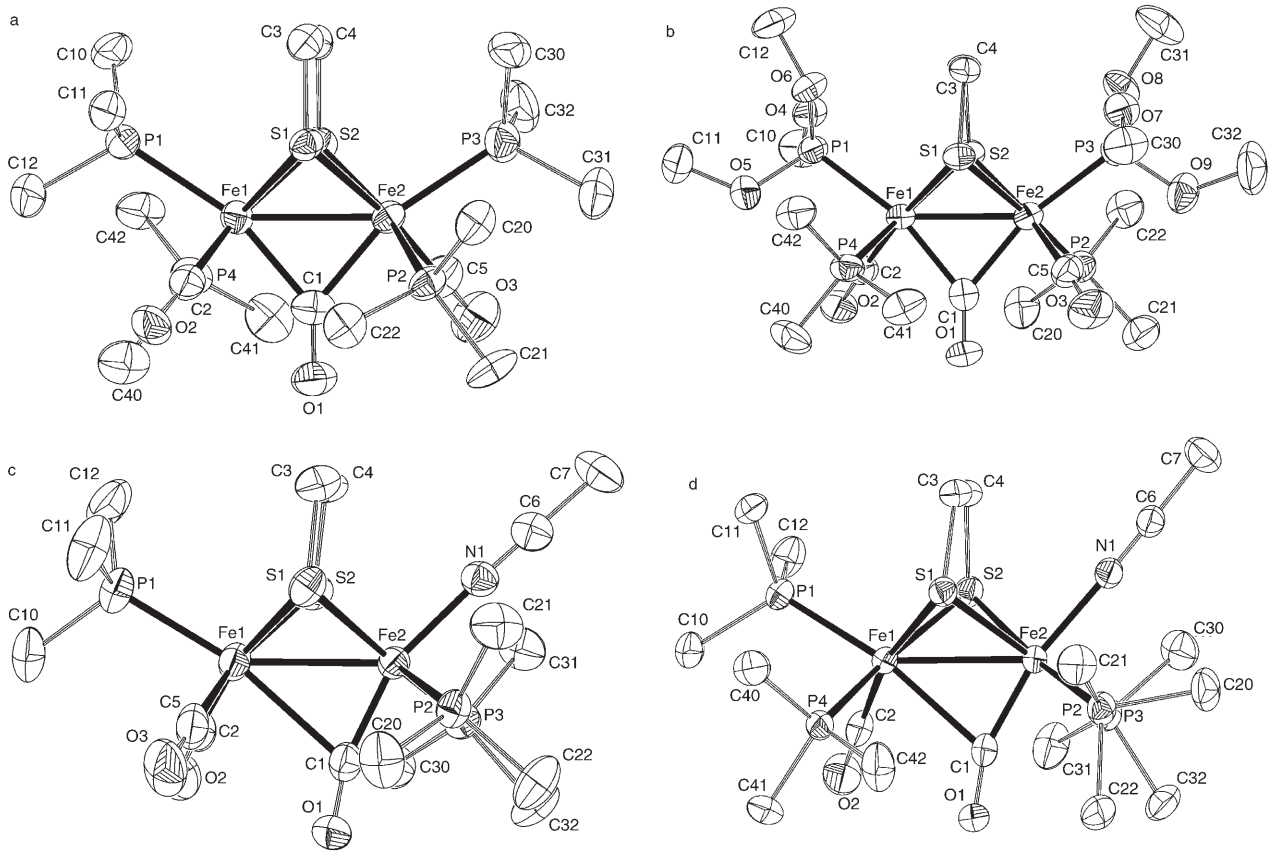

Figure 4. Molecular structures of the dications in: a) $[Fe_2(S_2C_2H_4)(\mu\text{-}CO)(CO)_2(PMe_3)_4](PF_6)_2$ (**3**), b) $[Fe_2(S_2C_2H_4)(\mu\text{-}CO)(CO)_2(PMe_3)_2(P(OMe)_3)_2](PF_6)_2$ (**4**), c) $[Fe_2(S_2C_2H_4)(\mu\text{-}CO)(CO)_2(PMe_3)_3(MeCN)](PF_6)_2$ (**5**), and d) $[Fe_2(S_2C_2H_4)(\mu\text{-}CO)(CO)(PMe_3)_4(MeCN)](PF_6)_2$ (**6**). Displacement ellipsoids are drawn at the 50% level. Hydrogen atoms have been omitted for clarity.

Table 2. Selected bond lengths [Å] and angles [°] for complexes **3**–**6**.

	3	**4**	**5**	**6**
Fe1–Fe2	2.5271(15)	2.5135(12)	2.5652(10)	2.6006(7)
Fe1–C1	1.957(8)	1.970(6)	2.407(4)	2.322(3)
Fe2–C1	1.960(9)	1.996(6)	1.775(4)	1.779(3)
Fe1–C2	1.757(10)	1.801(6)	1.808(5)	1.764(3)
Fe1–P1	2.285(2)	2.2002(17)	2.2235(13)	2.2295(9)
Fe2–P2	2.296(2)	2.2819(18)	2.2918(12)	2.3055(10)
Fe2–P3	2.276(3)	2.2006(18)	2.2934(13)	2.2861(9)
C1–O1	1.183(9)	1.161(7)	1.157(5)	1.172(3)
C2–O2	1.182(9)	1.122(7)	1.139(6)	1.154(3)
Fe2-Fe1-C1	49.9(3)	51.13(18)	41.68(10)	41.91(7)
Fe1-Fe2-C1	49.8(2)	50.20(18)	64.38(13)	60.64(9)
Fe1-C1-O1	140.3(7)	141.4(5)	121.1(3)	122.3(2)
Fe2-C1-O1	139.3(7)	140.0(5)	165.0(4)	160.0(2)
P1-Fe1-C1	162.3(3)	164.78(18)	168.56(11)	166.67(8)
P3-Fe2-C1	161.1(3)	165.45(18)	81.63(14)	82.85(9)
Fe2-Fe1-P1	144.94(8)	142.45(6)	149.28(5)	147.31(3)
Fe1-Fe2-P3	145.69(8)	142.97(6)	116.88(4)	115.43(3)

In the MeCN adducts, the geometry around the Fe bearing the MeCN ligand is distorted from octahedral, based on the angles ∢N1-Fe2-C1 of 160.34(16)° (**5**) and 168.14(11)° (**6**). The distortion is localized in the *semi*bridging CO ligand, as ∢N1-Fe2-$P_{2,3}$ and ∢N1-Fe2-$S_{1,2}$ are all ≈90°. The geometry around Fe1 is also distorted octahedral, due to the axial PMe_3 ligands, reflected in ∢P1-Fe1-$S_{1,2}$ of ≈100°. This disorder presumably arises from steric hindrance, as observed before in $[Fe_2(S_2C_2H_4)(\mu\text{-}CO)(CN)_2(CO)_2(PPh_3)_2]$.[23]

Conclusion

Oxidation of $[Fe_2(S_2C_2H_4)(CO)_4(PMe_3)_2]$ (**1**) with $[FeCp_2]PF_6$ followed by the low-temperature addition of phosphane ligands resulted in a series of diferrous–dithiolates containing either three or four phosphorus ligands. The reaction apparently occurs via the intermediacy of $\mathbf{1}^{2+}$, which was detected by in situ IR spectroscopy. The ligand addition reactions proceeded with high stereoselectivity to yield well-defined compounds, which is notable given the large variety of isomers possible. Also, despite the use of excess ligand (three equivalents), only two additional phosphorus ligands (PMe_3, $P(OMe)_3$) were incor-

porated, presumably because of steric hindrance. Compounds **2** and **3** were reactive toward further substitution by MeCN. Similar labile terminal CO coordination as seen in **2** allowed for photolytic dissociation of an axial CO ligand from H_{ox}^{CO}.[26,29] The added MeCN occupied the site *trans* to the Fe–Fe bond, reminiscent of the vacant site proposed for the H_{red} state of the Fe-only hydrogenases active site.[30] The lability of the MeCN ligand merits further attention.

The analogy between our model compounds and the H_{red} state of the Fe-only hydrogenase active site is reinforced by the coordination of the μ-CO ligand, which in **5** and **6** is highly asymmetrically bound. The effect is more pronounced in these two compounds than in the previously reported diferrous–dithiolates, for example, $[Fe_2(S_2C_2H_4)(\mu\text{-}CO)(CN)_2(CO)_2(PPh_3)_2]$, in which $\Delta(Fe\text{–}\mu C) = 0.295$ Å (Table 3).[23] The bending of the μ-CO ligands in **5** and **6** is evident from the angles ∢Fe2-C1-O1 of 165.0(4) (**5**) and 160.0(2)° (**6**), which Crabtree[31] has classified as "bent semibridging".[32,33] Cotton described semibridging CO coordination "as a means for a metal atom, otherwise tending to be excessively negative, to transfer electron density to a CO group on a less negatively charged metal atom."[34] In compounds **5** and **6**, however, the electron-rich iron center would appear to be Fe2, which bears the MeCN ligand. Highly relevant to our findings are the results of Adams, who has also uncovered bent semibridging CO ligands in the unsymmetrically substituted d^6–d^6 species $[Mn_2(S_2C_2H_4)(\mu\text{-}CO)(CO)_{6-x}(PMe_2Ph)_x]$ ($x = 1, 2$).[35] As in **5** and **6**, the μ-CO ligand in these manganese species is more tightly bonded to the metal bearing the fewer terminal CO ligands.

IR spectroscopic analysis showed that the $\nu_{\mu\text{-CO}}$ in the novel diferrous–dithiolates ranges from 1907 cm^{-1} in **5** down to 1840 cm^{-1} in **3**, for a $\Delta\nu$ of 67 cm^{-1}. This work further demonstrates the strong effect of the *trans*-coordinated ligands μ-CO and may therefore guide the development of functional models of the Fe-only hydrogenases.

Table 3. Fe–μC bond lengths for selected Fe_2 compounds featuring μ-CO and μ-CNMe ligands.

	Fe1–C1	Fe2–C1	ΔFe–C	Ref.
$[Fe_2(S_2C_2H_4)(\mu\text{-}CNMe)(CNMe)_6]^{2+}$	2.078(5)	2.078(5)	0	[15]
$[Fe_2(S_2C_3H_6)(\mu\text{-}CNMe)(CNMe)_6]^{2+}$	2.300(5)	1.952(5)	0.348	[15]
$[Fe_2(S_2C_3H_6)(\mu\text{-}CNMe)(CO)(CNMe)_5]^{2+}$	2.381(4)	1.916(4)	0.465	[22]
$[Fe_2(S_2C_3H_6)(\mu\text{-}CO)(CNMe)_6]^{2+}$	2.042(4)	1.947(4)	0.095	[22]
$[Fe_2(S_2C_2H_4)(\mu\text{-}CO)(CN\mathit{t}Bu)_6]^{2+}$	2.061(3)	1.933(3)	0.128	[22]
$Fe_2(S_2C_2H_4)(\mu\text{-}CO)(CN)_2(CO)_2(PPh_3)_2$	2.148(7)	1.853(7)	0.295	[22]
$[Fe_2(S_2C_2H_4)(\mu\text{-}CO)(CO)_2(PMe_3)_3(MeCN)]^{2+}$ (**5**)	2.407(4)	1.775(4)	0.632	this work
$[Fe_2(S_2C_2H_4)(\mu\text{-}CO)(CO)(PMe_3)_4(MeCN)]^{2+}$ (**6**)	2.322(3)	1.779(3)	0.543	this work
$Fe(bipy)(CO)_3(\mu\text{-}CO)Fe(CO)_3$	2.37	1.80	0.57	[34]
$Fe(CO)_2(\eta^2,\eta^4\text{-}C_4H_4)(\mu\text{-}CO)Fe(CO)_3$	2.508(4)	1.779(7)	0.729	[36–38]
$[Fe(C_5H_5)(CO)(\eta^1,\eta^4\text{-}CHC(CH_3)C(CH_3)C(O))(\mu\text{-}CO)Fe(C_5H_5)]^+$	2.091(13)	1.847(13)	0.244	[39]

Experimental Section

All manipulations were carried out under nitrogen using standard Schlenk techniques. Chemicals were purchased from Aldrich and solvents were either HPLC-grade from an argon-flushed column, packed with aluminum oxide, or distilled under nitrogen over an appropriate drying agent prior to use. Nitromethane was purified according to literature procedures.[40] NMR spectra were recorded at room temperature on a Varian Mercury 500 MHz spectrometer. Chemical shifts are given in ppm and spectra are referenced to $CDCl_3$ (^1H, $^{13}C\{^1H\}$) or 85% H_3PO_4 ($^{31}P\{^1H\}$). FT-IR spectra were taken on a Mattson Infinity Gold FTIR spectrometer. Real-time ATR-IR spectra were recorded on a Mettler-Toledo ReactIR® 4000 spectrometer. $[Fe_2(S_2C_2H_4)(CO)_4(PMe_3)_2]$ and $[Fe_2(S_2C_2H_4)(CO)_4(P(OMe)_3)_2]$ were prepared by thermal substitution as generally described.[41] PMe_3 was distilled on a high-vacuum line prior to use.

$[Fe_2(S_2C_2H_4)(\mu\text{-}CO)(CO)_3(PMe_3)_3](PF_6)_2$ (2): A solution of **1** (0.11 g, 0.24 mmol) in purified $MeNO_2$ (30 mL), saturated with CO and cooled to −30 °C, was treated with a solution of $[FeCp_2]PF_6$[42] (0.16 g, 0.49 mmol) in $MeNO_2$ (10 mL), followed after 20 min by addition of PMe_3 (0.025 mL, 0.24 mmol) in $MeNO_2$ (5 mL). After an additional 20 min, the mixture was allowed to warm to ambient temperature, and the solvent was removed in vacuo. The crude solid was washed with hexanes to remove ferrocene, leaving **2** as a dark red solid. Yield: 0.15 g (0.18 mmol, 77%). Alternatively, the BF_4^- salt of **2** could be prepared analogously, using CH_2Cl_2 in place of $MeNO_2$ and $[FeCp_2]BF_4$ as the oxidant. The product precipitated as a purple-red solid. ^1H NMR (500 MHz, CD_3NO_2): $\delta =$ 3.52 (m, 2H; SCH_2CH_2S), 3.29 (m, 2H; SCH_2CH_2S), 2.03 (d, $J_{PH} = 11$ Hz, 18H; $P(CH_3)_3$), 1.85 ppm (d, $J_{PH} =$ 11 Hz, 18H; $P(CH_3)_3$); ^{31}P NMR (202 MHz, CD_3NO_2): $\delta = 39.8$ (t, $^3J_{PP} =$ 6 Hz, 1P), 24.0 (d, $^3J_{PP} = 6$ Hz, 2P), −143.8 ppm (heptet, 2P; PF_6); FT-IR (CH_3NO_2): $\tilde{\nu} = 2055$ (s), 2019 (s) (Fe(*CO*)), 1942 cm^{-1} (w) (Fe(μ-*CO*)); ESI-MS (CH_3NO_2): m/z: 689.1 $[M+PF_6]^+$.

$[Fe_2(S_2C_2H_4)(\mu\text{-}CO)(CO)_2(PMe_3)_4](PF_6)_2$ (3): A solution of **1** (0.12 g, 0.26 mmol) in purified $MeNO_2$ (30 mL), saturated with CO and cooled to −30 °C, was treated with a solution of $[FeCp_2]PF_6$ (0.24 g, 0.74 mmol) in $MeNO_2$ (10 mL) followed after 20 min by addition of PMe_3 (0.54 mL, 0.52 mmol) in $MeNO_2$ (5 mL). The standard workup described above afforded **3** as dark red diamondoid crystals. Yield: 0.19 g (0.22 mmol, 84%). ^1H NMR (500 MHz, CD_3NO_2): $\delta = 3.42$ (br m, 2H; SCH_2CH_2S), 3.07 (br m, 2H; SCH_2CH_2S), 2.04 (d, $J_{PH} = 10$ Hz, 18H; $P(CH_3)_3$), 1.71 ppm (d, $J_{PH} = 10$ Hz, 18H; $P(CH_3)_3$); ^{31}P NMR (202 MHz, CD_3NO_2): $\delta = 21.0$ (dd, $^2J_{PP} = 49$ Hz, $^3J_{PP} = 6$ Hz, 2P), 19.7 (d, $^2J_{PP} = 49$ Hz, $^3J_{PP} =$ 6 Hz, 2P), −143.8 ppm (septet, 2P; PF_6); FT-IR (CH_3NO_2): $\tilde{\nu} = 2013$ (sh, m), 2001 (s) (Fe(*CO*)), 1840 cm^{-1} (w) (Fe(μ-*CO*)); elemental analysis calcd (%) for $C_{17}H_{40}F_{12}Fe_2O_3P_6S_2$: C 23.15, H 4.57; found: C 23.19, H 4.53; ESI-MS (CH_3NO_2): m/z: 737.2 $[M+PF_6]^+$.

$[Fe_2(S_2C_2H_4)(\mu\text{-}CO)(CO)_2(PMe_3)_2(P(OMe)_3)_2](PF_6)_2$ (4): A solution of **1** (0.10 g, 0.22 mmol) in MeCN (30 mL), saturated with CO and cooled to −40 °C, was treated with a solution of $[FeCp_2]PF_6$ (0.16 g, 0.49 mmol) in MeCN (10 mL). After stirring for approximately 2 min, $P(OMe)_3$ (0.080 mL, 0.64 mmol) was then added. The reaction mixture was stirred for an additional 20 min at −40 °C before being allowed to warm to room temperature. Solvent was removed in vacuo to leave a red solid, which was washed with hexanes to remove ferrocene. The residue was extracted into CH_2Cl_2 (15 mL), and this solution was layered with hexane (50 mL). Slow diffusion overnight at room temperature yielded red needlelike crystals for **4**. Yield: 0.15 g (0.15 mmol, 70%). When a solution of **4** in MeCN was heated to 50 °C for 36 h, complete conversion to the corresponding solvento adduct $[Fe_2(S_2C_2H_4)(\mu\text{-}CO)(CO)(PMe_3)_2(P(OMe)_3)_2(MeCN)](PF_6)_2$ was observed by IR spectroscopy. ^1H NMR (500 MHz, CD_3CN): $\delta = 4.02$ (d, $J_{PH} = 11$ Hz, 18H; $P(OCH_3)_3$), 3.12 (m, 2H; SCH_2CH_2S), 2.95 (m, 2H; SCH_2CH_2S), 1.61 ppm (d, $J_{PH} = 11$ Hz, 18H; $P(CH_3)_3$); ^{31}P NMR (202 MHz, CD_3CN): $\delta = 143.4$ (dd, $^1J_{PP} = 89$ Hz, $^2J_{PP} =$

6 Hz, 2P(OMe)$_3$), 21.3 (d, $^1J_{P,P}=89$ Hz, $^1J_{P,P}=6$ Hz; 2PMe$_3$), −143.8 ppm (heptet, 2P; PF$_6$); FT-IR (CH$_3$CN): $\tilde{\nu}=2028$ (sh, m), 2015 (s) (Fe(*CO*)), 1863 cm^{-1} (w) (Fe(μ-*CO*)); MeCN adduct: $\tilde{\nu}=1990$, 1898 cm^{-1}; FT-IR (CH$_3$CN): ν 2028 (sh, m), 2015 (s) (Fe(*CO*)), 1863 cm^{-1} (w) (Fe(μ-*CO*)); elemental analysis calcd (%) for $C_{17}H_{40}F_{12}Fe_2O_9P_6S_2$: C 20.87, H 4.12; found: C 20.34, H 3.96; ESI-MS (CH$_2$Cl$_2$): *m*/*z*: 833.1 $[M+PF_6]^+$.

[Fe$_2$(S$_2$C$_2$H$_4$)(μ-CO)(CO)$_2$(PMe$_3$)$_3$(MeCN)](PF$_6$)$_2$ (5): A solution of **1** (0.45 g (0.96 mmol) in MeCN (30 mL), saturated with CO and cooled to −40 °C, was treated with a solution of [FeCp$_2$]PF$_6$ (0.73 g, 2.21 mmol) in MeCN (10 mL). After 20 min, a solution of PMe$_3$ (0.10 mL, 0.96 mmol) in MeCN (5 mL) was added. IR spectra (−40 °C) are consistent with the intermediacy of **3**. After 20 min, the mixture was allowed to warm up to ambient temperature. Solvent was removed in vacuo to leave a crude green solid, which was washed with hexanes to remove ferrocene. The residue was extracted into MeCN (15 mL), and this extract was layered with Et$_2$O (50 mL). Slow diffusion overnight at room temperature yielded dark-green diamondoid crystals. Yield: 0.71 g (0.84 mmol, 87 %). Upon stirring **5** in neat EtCN for 2 h, we observed exchange of coordinated MeCN for coordinated EtCN in the ^{31}P NMR spectrum of the resulting green solid, with overlaying triplets at $\delta=35.9$ ppm, but separated doublets at $\delta=27.6$ (MeCN) and 26.9 ppm (EtCN). Compound **5** was also cleanly obtained when a solution of **2** in MeCN was left standing for ≈2 h. ^{1}H NMR (500 MHz, CD$_3$CN): $\delta=3.12$ (m, 2H; SC*H*$_2$C*H*$_2$S), 2.88 (m, 2H; SC*H*$_2$C*H*$_2$S), 2.66 (t, $J_{P,H}=3$ Hz, 3H; Fe-NCC*H*$_3$), 1.86 (d, $J_{P,H}=11$ Hz, 9H; P$_{ax}$(C*H*$_3$)$_3$), 1.58 ppm (d, $J_{P,H}=11$ Hz, 18H; P$_{ba}$(C*H*$_3$)$_3$); ^{13}C NMR (125 MHz, CD$_3$CN): $\delta=218.2$ (dt, $^2J_{P,C}=41$ Hz, $^2J_{P,C}=6$ Hz; μ-CO), 205.4 (d, $^2J_{P,C}=22$ Hz; basal CO), 137.1 (s, N*C*CH$_3$), 36.1 (s, $^3J_{P,C}=5$ Hz; SCH$_2$CH$_2$S), 20.0 (d, $^1J_{P,C}=34$ Hz; P(*C*H$_3$)), 15.4 (t, $^1J_{P,C}=15$ Hz; P-(*C*H$_3$)), 15.1 (t, $^1J_{P,C}=15$ Hz; P(*C*H$_3$)), 5.2 ppm (s; NC*C*H$_3$). ^{31}P NMR (202 MHz, CD$_3$CN): $\delta=35.9$ (t, $^3J_{P,P}=6$ Hz, 1P), 27.5 (d, $^3J_{P,P}=6$ Hz, 2P), −143.8 (septet, 2P; PF$_6$); FT-IR (CH$_3$CN): $\tilde{\nu}=2053$ (s), 2006 (s) (Fe(*CO*)), 1908 cm^{-1} (w) (Fe(μ-*CO*)); elemental analysis calcd (%) for $C_{16}H_{34}F_{12}Fe_2NO_3P_5S_2$: C 22.69, H 4.05, N 1.65; found: C 22.53, H 4.04, N 1.66; ESI-MS (CH$_3$CN): *m*/*z*: 702.1 $[M+PF_6]^+$.

[Fe$_2$(S$_2$C$_2$H$_4$)(μ-CO)(CO)$_2$(PMe$_3$)$_3$(EtCN)](PF$_6$)$_2$: A solution of **1** (0.15 g, 0.32 mmol) in unpurified MeNO$_2$ (30 mL), saturated with CO and cooled to −30 °C, was treated with a solution of [FeCp$_2$]PF$_6$ (0.24 g, 0.74 mmol) in of Me$_3$NO$_2$ (10 mL), followed, after stirring for 20 min, by the addition of a solution of PMe$_3$ (0.033 mL, 0.32 mmol) in MeNO$_2$ (5 mL). After an additional 20 min, the mixture was allowed to warm to ambient temperature, and the solvent was removed in vacuo. The crude green solid was washed with hexanes to remove ferrocene and the residue was dissolved in MeNO$_2$ (15 mL), and this solution was layered with Et$_2$O (15 mL). Slow diffusion was allowed to proceed overnight at room temperature to yield a dark-green solid. Single crystals were grown from MeNO$_2$/Et$_2$O and the molecular structure was elucidated by X-ray crystallography as isostructural to **4**. Yield: 0.21 g (0.25 mmol, 78 %). ^{1}H NMR (500 MHz, CD$_3$CN): $\delta=3.08$ (m, 2H; SC*H*$_2$C*H*$_2$S), 3.04 (m, 2H; Fe-NCC*H*$_2$CH$_3$), 2.88 (m, 2H; SC*H*$_2$C*H*$_2$S), 1.86 (d, $J_{P,H}=11$ Hz, 9H; P$_{ax}$(C*H*$_3$)$_3$), 1.58 (d, $J_{P,H}=11$ Hz, 18H; P$_{ba}$(C*H*$_3$)$_3$), 1.40 ppm (t, $J_{P,H}=3$ Hz, 3H; Fe-NCCH$_2$C*H*$_3$); ^{31}P NMR (202 MHz, CD$_3$CN): $\delta=35.9$ (t, $^3J_{P,P}=6$ Hz, 1P), 26.9 (d, $^3J_{P,P}=6$ Hz, 2P), −143.8 ppm (septet, 2P; PF$_6$); FT-IR (CH$_3$CN): $\tilde{\nu}=2054$ (s), 2007 (s) (Fe(*CO*)), 1909 cm^{-1} (w) (Fe(μ-*CO*)); ESI-MS (CH$_3$CN): *m*/*z*: 716.1 $[M+PF_6]^+$.

[Fe$_2$(S$_2$C$_2$H$_4$)(μ-CO)(CO)$_2$(PMe$_3$)$_2$(PMe$_2$Ph)(MeCN)](PF$_6$)$_2$: A solution of **1** (0.11 g, 0.24 mmol) in MeCN (25 mL), saturated with CO and cooled to −40 °C, was treated with a solution of [FeCp$_2$]PF$_6$ (0.18 g, 0.54 mmol) in MeCN (10 mL), followed after stirring for approximately 2 min by the addition of PMe$_2$Ph (0.033 mL, 0.24 mmol). The reaction mixture was stirred for an additional 20 min at −40 °C before being allowed to warm ambient temperature. Solvent was removed in vacuo, and the crude product was washed with hexane to remove ferrocene, yielding a green solid that was spectroscopically pure. ^{31}P NMR (202 MHz, CD$_3$CN): $\delta=35.8$ (t, $^3J_{P,P}=6$ Hz; axial PMe$_3$), 28.6 (dd, $^2J_{P,P}=25$ Hz, $^3J_{P,P}=6$ Hz; basal PMe$_2$Ph), 26.1 (dd, $^2J_{P,P}=25$ Hz, $^3J_{P,P}=6$ Hz; basal PMe$_3$), −143.8 ppm (septet, 2P; PF$_6$); FT-IR (CH$_3$CN): $\tilde{\nu}=2053$ (s), 2007 (s) (Fe(*CO*)), 1907 cm^{-1} (w) (Fe(μ-*CO*)); ESI-MS (CH$_3$CN): *m*/*z*: 764.1 $[M+PF_6]^+$.

[Fe$_2$(S$_2$C$_2$H$_4$)(μ-CO)(CO)(PMe$_3$)$_4$(MeCN)](PF$_6$)$_2$ (6): A solution of **1** (0.35 g, 0.75 mmol) in MeCN (30 mL), saturated with CO and cooled to −40 °C, was treated with a solution of [FeCp$_2$]PF$_6$ (0.57 g, 1.71 mmol) in MeCN (10 mL), followed, after 20 min, with a solution of PMe$_3$ (0.23 mL, 2.24 mmol) in MeCN (10 mL). For a sample taken after 15 min, the IR spectrum matched that observed for **3**. After an additional 20 min, the reaction mixture was allowed to warm up to ambient temperature. Solvent was removed in vacuo to leave a crude red solid. The product was washed with hexanes to remove ferrocene. The residue was dissolved in MeCN (15 mL) and layered with of Et$_2$O (50 mL). Slow diffusion overnight at room temperature yielded **6** as dark-red diamond-shaped crystals. Yield: 0.56 g (84 %, 0.63 mmol). Compound **6** was also cleanly obtained upon solvolysis of **3** in MeCN for ≈20 h. Alternatively, addition of PMe$_3$ to a solution of **5** in MeCN led to **3** initially. Subsequent solvolysis of this compound yielded intermediate **A**, giving **6** as the final isolable product. The rate of conversion from **5** to **6** was dependent on solvent (MeNO$_2$ or MeCN). ^{1}H NMR (500 MHz, CD$_3$CN): $\delta=3.20$ (m, 1H; SC*H*$_2$C*H*$_2$S), 2.93 (m, 1H; SC*H*$_2$C*H*$_2$S), 2.81 (m, 2H; SC*H*$_2$C*H*$_2$S), 2.69 (t, $J_{P,H}=2$ Hz, 3H; Fe-NCC*H*$_3$), 1.67 (d, $J_{P,H}=11$ Hz, 9H; P(C*H*$_3$)$_3$ (P$_1$)), 1.58 (d, $J_{P,H}=11$ Hz, 18H; P(C*H*$_3$)$_3$ (P$_2$,P$_4$)), 1.47 ppm (d, $J_{P,H}=11$ Hz, 9H; P(C*H*$_3$)$_3$ (P$_3$)); ^{1}H NMR (500 MHz, CD$_3$NO$_2$): $\delta=3.31$ (m, 1H; SC*H*$_2$C*H*$_2$S), 3.01 (m, 1H; SC*H*$_2$C*H*$_2$S), 2.94 (m, 2H; SC*H*$_2$C*H*$_2$S), 2.82 (t, $J_{P,H}=2$ Hz, 3H; Fe-NCC*H*$_3$), 1.77 (d, $J_{P,H}=11$ Hz, 9H; P(C*H*$_3$)$_3$ (P$_1$)), 1.68 (d, $J_{P,H}=11$ Hz, 18H; P(C*H*$_3$)$_3$ (P$_2$,P$_4$)), 1.56 ppm (d, $J_{P,H}=11$ Hz, 9H; P(C*H*$_3$)$_3$ (P$_3$)); ^{13}C NMR (125 MHz, CD$_3$CN): $\delta=223.6$ (dddd, $^2J_{P,C}=38$ Hz, $^2J_{P,C}=30$ Hz, $^2J_{P,C}=6$ Hz, $^2J_{P,C}=3$ Hz; μ-CO), 212.3 (dd, $^2J_{P,C}=32$ Hz, $^2J_{P,C}=19$ Hz; basal CO), 137.5 (s; N*C*CH$_3$), 37.3 (d, $^3J_{P,C}=5$ Hz; S*C*H$_2$CH$_2$S), 33.3 (dd, $^3J_{P,C}=11$ Hz, $^3J_{P,C}=5$ Hz; SCH$_2$*C*H$_2$S), 20.2 (d, $^1J_{P,C}=31$ Hz; P(*C*H$_3$)), 17.8 (d, $^1J_{P,C}=30$ Hz; P(*C*H$_3$)), 16.5 (d, $^1J_{P,C}=31$ Hz; P(*C*H$_3$)), 14.1 (d, $^1J_{P,C}=31$ Hz; P(*C*H$_3$)), 4.8 ppm (s, NC*C*H$_3$); ^{31}P NMR (202 MHz, CD$_3$CN): $\delta=32.7$ (ddd, $^2J_{P,P}=41$ Hz, $^3J_{P,P}=6$ Hz, $^3J_{P,P}=4.5$ Hz, 1P; P$_1$), 24.0 (dd, $^2J_{P,P}=29$ Hz, $^3J_{P,P}=6$ Hz, 1P; P$_3$), 14.1 (d, $^2J_{P,P}=29$ Hz, 1P; P$_2$), 13.5 (d, $^2J_{P,P}=41$ Hz, 1P; P$_4$), −143.8 ppm (heptet, 2P; PF$_6$); ^{31}P NMR (202 MHz, CD$_3$NO$_2$): $\delta=32.3$ (ddd, $^2J_{P,P}=41$ Hz, $^3J_{P,P}=6$ Hz, $^3J_{P,P}=3$ Hz, 1P; P$_1$), 24.5 (ddd, $^2J_{P,P}=29$ Hz, $^3J_{P,P}=6$ Hz, $^3J_{P,P}=3$ Hz, 1P; P$_3$), 14.6 (d, $^2J_{P,P}=29$ Hz, 1P; P$_2$), 14.1 (d, $^2J_{P,P}=41$ Hz, 1P; P$_4$), −143.8 ppm (heptet, 2P; PF$_6$); FT-IR (CH$_3$CN): $\tilde{\nu}=1969$ (s) (Fe(*CO*)), 1878 cm^{-1} (w) (Fe(μ-*CO*)); elemental analysis calcd (%) for $C_{18}H_{43}F_{12}Fe_2NO_2P_6S_2$: C 24.15, H 4.84, N 1.56; found: C 24.51, H 4.97, N 2.26; ESI-MS (CH$_3$CN): *m*/*z*: 750.0 $[M+PF_6]^+$. Product **A**, which was initially formed by addition of PMe$_3$ to **5** in MeCN or MeNO$_2$, as monitored by ^{31}P NMR spectroscopy, was characterized by four inequivalent phosphane-groups at $\delta=31.0$ (dd, $J_{P,P}=45$, 5 Hz), 17.5 (dd, $J_{P,P}=22$, 5 Hz), 13.4 (d, $J_{P,P}=45$ Hz), and 8.4 ppm (d, $J_{P,P}=22$ Hz). In the ^{1}H NMR spectrum, four doublets ($\delta=1.88$, 1.81, 1.71, and 1.66 ppm) were assigned to this species. From these spectroscopic data, we propose that this species **A** is an isomer of **6**.

X-ray crystallography: Table 4 gives details of the data collection and refinement. Structures were phased by direct methods.[43] The proposed model for **3** includes two disordered sites for the first anion, three disordered sites for the second anion, and two disordered sites for the solvate molecule. The proposed model for **4** includes two host molecules in the asymmetric unit, and one ordered and three disordered anion sites. Contributions from the disordered solvate molecule were removed from the diffraction data using the bypass procedure in PLATON.[44] The proposed model for **5** includes two molecules in the unit cell, two disordered sites for the first, second and third anion, three disordered sites for the fourth anion, and two disordered sites for the second solvate molecule. The proposed model for **6** includes two disordered sites for the second anion, and two disordered sites for the second solvate molecule. Anion molecules were refined as idealized rigid groups. Methyl H atom positions, R-CH$_3$, were optimized by rotation about R−C bonds with idealized C−H, R−H, and H−H distances. Remaining H atoms were included as riding idealized contributors. The space group choice in each case was confirmed by successful convergence of the full-matrix least-squares refinement on F^2.[43] CCDC-276468–CCDC-276471 contain the supplementary crystallographic data for this paper. These data can be obtained free of charge from The Cambridge Crystallographic Data Centre via www.ccdc.cam.ac.uk/data_request/cif.

Table 4. Selected crystallographic data for complexes **3**–**6**.

	3	**4**	**5**	**6**
formula	$C_{18}H_{43}F_{12}Fe_2NO_5P_6S_2$	$C_{69}H_{162}Cl_2F_{48}Fe_8O_{36}P_{24}S_8$	$C_{16}H_{34}F_{12}Fe_2NO_3P_5S_2$	$C_{22}H_{49}F_{12}Fe_2N_3O_2P_6S_2$
M_r [g mol^{-1}]	943.17	3997.45	847.11	977.28
T [K]	193(2)	193(2)	193(2)	193(2)
λ [Å]	0.71073	0.71073	0.71073	0.71073
crystal size [mm^3]	0.55×0.45×0.32	0.60×0.36×0.04	0.72×0.26×0.24	0.40×0.15×0.10
crystal system	monoclinic	orthorhombic	orthorhombic	monoclinic
space group	*Cc*	*Pccn*	*Pbca*	$P2_1/c$
a [Å]	11.027(3)	23.192(3)	17.420(5)	10.249(3)
b [Å]	22.164(6)	47.253(6)	15.966(4)	34.551(9)
c [Å]	15.495(4)	14.0307(18)	47.354(13)	11.889(3)
α [°]	90	90	90	90
β [°]	102.866(5)	90	90	93.699(4)
γ [°]	90	90	90	90
V [A^3]	3692.0(17)	15376(3)	13170(6)	4201.1(19)
Z	4	4	16	4
ρ_{calcd} [g cm^{-3}]	1.697	1.727	1.709	1.545
μ ($Mo_{K\alpha}$) [mm^{-1}]	1.250	1.246	1.341	1.098
F(000)	1920	8104	6848	2000
σ range	1.84–25.38	1.72–25.31	2.59–27.34	1.81–26.37
total reflns	14833	146272	133499	47735
independent reflns [R(int)]	6668 [0.0893]	13876 [0.0955]	14400 [0.0679]	8574 [0.0550]
absorption correction	integration	integration	integration	empirical
max/min transmission	0.9483/0.7405	0.9483/0.7405	0.9483/0.7405	0.7462/0.7039
parameters	584	992	945	550
goodness-of-fit on F^2	0.879	1.1049	1.020	1.0359
final R indices [$I>2\sigma(I)$]	$R1=0.0555$, $wR2=0.0959$	$R1=0.0742$, $wR2=0.1591$	$R1=0.0501$, $wR2=0.1051$	$R1=0.0383$, $wR2=0.0783$
R indices (all data)	$R1=0.1182$, $wR2=0.1101$	$R1=0.1074$, $wR2=0.1732$	$R1=0.0868$, $wR2=0.1175$	$R1=0.0629$, $wR2=0.0836$
largest diff. peak/hole [e Å^{-3}]	0.580/−0.339	1.209/−0.606	0.708/−0.510	0.409/−0.257

Acknowledgements

This work was supported by the US National Institutes of Health and, in part, by the U.S. Department of Energy (funding for the ReactIR® instrument). We thank Christine Boyke for helpful discussions, Aaron Justice for assistance with in situ IR measurements, and Terésa Prussak-Wieckowska for X-ray crystallographic analyses.

[1] H. Reihlen, A. von Friedolsheim, W. Ostwald, *Justus Liebigs Ann. Chem.* **1928**, *465*, 72–96.
[2] W. Hieber, P. Spacu, *Z. Anorg. Allg. Chem.* **1937**, *233*, 852–864.
[3] M. Frey, *ChemBioChem* **2002**, *3*, 153–160.
[4] Y. Nicolet, B. J. Lemon, J. C. Fontecilla-Camps, J. W. Peters, *Trends Biochem. Sci.* **2000**, *25*, 138–143.
[5] R. Cammack, M. Frey, R. Robson, *Hydrogen as a Fuel: Learning from Nature*, Taylor & Francis, London, **2001**.
[6] R. B. King, T. E. Bitterwolf, *Coord. Chem. Rev.* **2000**, *206–207*, 563–579.
[7] Y. Nicolet, A. L. de Lacey, X. Vernede, V. M. Fernandez, E. C. Hatchikian, J. C. Fontecilla-Camps, *J. Am. Chem. Soc.* **2001**, *123*, 1596–1601.
[8] M. Y. Darensbourg, E. J. Lyon, X. Zhao, I. P. Georgakaki, *Proc. Natl. Acad. Sci. USA* **2003**, *100*, 3683–3688.
[9] C. Tard, X. Liu, S. K. Ibrahim, M. Bruschi, L. De Gioia, S. C. Davies, X. Yang, L.-S. Wang, G. Sawers, C. J. Pickett, *Nature* **2005**, *433*, 610–614.
[10] F. Gloaguen, J. D. Lawrence, T. B. Rauchfuss, *J. Am. Chem. Soc.* **2001**, *123*, 9476–9477.
[11] F. Gloaguen, J. D. Lawrence, T. B. Rauchfuss, M. Bénard, M.-M. Rohmer, *Inorg. Chem.* **2002**, *41*, 6573–6582.
[12] L. Sun, B. Åkermark, S. Ott, *Coord. Chem. Rev.* **2005**, *249*, 1653–1663.
[13] W.-F. Liaw, N.-H. Lee, C.-H. Chen, C.-M. Lee, G.-H. Lee, S.-M. Peng, *J. Am. Chem. Soc.* **2000**, *122*, 488–494.
[14] W.-F. Liaw, W.-T. Tsai, H.-B. Gau, C.-M. Lee, S.-Y. Chou, W.-Y. Chen, G.-H. Lee, *Inorg. Chem.* **2003**, *42*, 2783–2788.
[15] J. D. Lawrence, T. B. Rauchfuss, S. R. Wilson, *Inorg. Chem.* **2002**, *41*, 6193–6195.
[16] C. T. Lam, M. Novotny, D. L. Lewis, S. J. Lippard, *Inorg. Chem.* **1978**, *17*, 2127–2133.
[17] J. A. Kovacs, J. K. Bashkin, R. H. Holm, *Polyhedron* **1987**, *6*, 1445–1456.
[18] J. L. Le Quere, F. Y. Petillon, J. E. Guerchais, L. Manojlovic-Muir, K. W. Muir, D. W. A. Sharp, *J. Organomet. Chem.* **1983**, *249*, 127–135.
[19] K. S. Bose, S. A. Chmielewski, P. A. Eldredge, E. Sinn, B. A. Averill, *J. Am. Chem. Soc.* **1989**, *111*, 8953–8954.
[20] S. E. Nefedov, A. A. Pasynskii, I. L. Eremenko, E. E. Stomakhina, A. I. Yanovskii, Y. T. Struchkov, *J. Organomet. Chem.* **1991**, *405*, 287–297.
[21] A. C. Filippou, W. Gruenleitner, *J. Organomet. Chem.* **1991**, *407*, 61–79.
[22] C. A. Boyke, T. B. Rauchfuss, S. R. Wilson, M.-M. Rohmer, M. Bénard, *J. Am. Chem. Soc.* **2004**, *126*, 15151–15160.
[23] C. A. Boyke, J. I. van der Vlugt, T. B. Rauchfuss, S. R. Wilson, G. Zampella, L. DeGioia, *J. Am. Chem. Soc.* **2005**, *127*, 11010–11018.
[24] M. Schmidt, S. M. Contakes, T. B. Rauchfuss, *J. Am. Chem. Soc.* **1999**, *121*, 9736–9737.
[25] J. C. Bardin, *Analusis* **1972**, *1*, 140–144.
[26] B. J. Lemon, J. W. Peters, *Biochemistry* **1999**, *38*, 12969–12973.
[27] F. A. Cotton, L. Kruczynski, B. A. Frenz, *J. Organomet. Chem.* **1978**, *160*, 93–100.
[28] F. A. Cotton, *Prog. Inorg. Chem.* **1976**, *21*, 1–28.
[29] B. J. Lemon, J. W. Peters, *J. Am. Chem. Soc.* **2000**, *122*, 3793–3794.
[30] A. L. De Lacey, C. Stadler, C. Cavazza, E. C. Hatchikian, V. M. Fernandez, *J. Am. Chem. Soc.* **2000**, *122*, 11232–11233.
[31] R. H. Crabtree, M. Lavin, *Inorg. Chem.* **1986**, *25*, 805–812.
[32] P. Macchi, L. Garlaschelli, A. Sironi, *J. Am. Chem. Soc.* **2002**, *124*, 14173–14184.
[33] H. F. Schaefer, R. B. King, *Pure Appl. Chem.* **2001**, *73*, 1059–1073.

[34] F. A. Cotton, J. M. Troup, *J. Am. Chem. Soc.* **1974**, *96*, 1233–1234.
[35] R. D. Adams, O. S. Kwon, M. D. Smith, *Isr. J. Chem.* **2001**, *41*, 197–206.
[36] G. Dettlaf, E. Weiss, *J. Organomet. Chem.* **1976**, *108*, 213–223.
[37] H. G. Raubenheimer, G. J. Kruger, L. Linford, *Inorg. Chim. Acta* **1988**, *150*, 173–176.
[38] F. Muller, I. M. Han, G. van Koten, K. Vrieze, D. Heijdenrijk, R. L. De Jong, M. C. Zoutberg, *Inorg. Chim. Acta* **1989**, *158*, 81–98.
[39] C. P. Casey, L. K. Woo, P. J. Fagan, R. E. Palermo, B. R. Adams, *Organometallics* **1987**, *6*, 447–454.
[40] J. F. Coetzee, T. H. Chang, *Pure Appl. Chem.* **1986**, *58*, 1541–1545.
[41] K. Fauvel, R. Mathieu, R. Poilblanc, *Inorg. Chem.* **1976**, *15*, 976–978.
[42] N. G. Connelly, W. E. Geiger, *Chem. Rev.* **1996**, *96*, 877–922.
[43] G. M. Sheldrick, SHELX-97–2: Program for Crystal Structure Solution and Refinement. 2001, University of Göttingen, Göttingen, Germany.
[44] A. L. Spek, *J. Appl. Cryst.* **2003**, *36*, 7–13.

Received: June 30, 2005
Published online: October 12, 2005

